Coexistence of the Meissner and vortex states on a nanoscale superconducting spherical shell

J. Tempere,[1,2] V. N. Gladilin,[1,3] I. F. Silvera,[2] J. T. Devreese,[1] and V. V. Moshchalkov[3]
[1]*TFVS, Universiteit Antwerpen, Groenenborgerlaan 171, 2020 Antwerpen, Belgium*
[2]*Lyman Laboratory of Physics, Harvard University, Cambridge, Massachusetts 02138, USA*
[3]*INPAC, K. U. Leuven, Celestijnenlaan 200 D, B-3001 Leuven, Belgium*
(Received 10 January 2009; revised manuscript received 16 March 2009; published 17 April 2009)

We show that on superconducting spherical nanoshells, the coexistence of the Meissner state with a variety of vortex patterns drives the phase transition to higher magnetic fields. The spherical geometry leads to a Magnus-Lorentz force pushing the nucleating vortices and antivortices toward the poles, overcoming local pinning centers, preventing vortex-antivortex recombination, and leading to the appearance of a Meissner belt around the sphere equator. In sufficiently small and thin spherical shells paramagnetic vortex states can be stable, enabling spatial separation of freely moving shells with different radii and vorticity in an inhomogeneous external magnetic field.

DOI: 10.1103/PhysRevB.79.134516 PACS number(s): 74.78.Na, 74.20.De, 74.25.Dw, 74.25.Qt

I. INTRODUCTION

Controlling and understanding vortex behavior and creating a guided vortex (fluxon) motion in superconductors are crucial for developing fluxonics devices.[1–7] Several key experiments have demonstrated how different vortex patterns can be created and guided in mesoscopic and nanoscopic superconductors.[1–4] These breakthroughs in the pursuit of "fluxonics" have focused on hybrid superconductor/ferromagnet nanosystems[1,2] or on the use of nanostructured superconductors.[3,4,8] Here, we investigate how the geometry (curvature and topology) of the superconducting layer rather than the patterning can be used to control flux. Curvature and surface topology, which are known to strongly affect, e.g., charge ordering and the dynamics of defects on spherical surfaces,[9,10] have a profound influence also on the vortex behavior in superconducting layers. We focus on the vortex behavior in spherical nanoshells. These are nanoparticles consisting of a dielectric core of typically 50–200 nm in radius, coated by a 5–20 nm thin metallic shell.[11] Thermodynamically stable vortex states in nanoshells as well as the dynamics of vortex trapping and releasing are investigated within the Ginzburg-Landau formalism applied to a spherical surface. Results of both variational analysis and numerical solutions are presented.

In the Ginzburg-Landau formalism, superconductors are described by a macroscopic wave function $\psi=|\psi|\exp(i\varphi)$ that couples to the electromagnetic field and takes the role of the complex order parameter for the superconducting phase. The modulus square of the order parameter $|\psi|^2$ corresponds to the density of Cooper pairs, whereas the gradient of its phase φ defines the supercurrent. We focus on thin superconducting nanoshells with a shell thickness $\mathcal{W}$ smaller than the correlation length ξ (that also defines the vortex core size). This requirement simplifies the treatment in two important ways. First, the order parameter will be constant in the shell along the radial direction, so ψ will only depend on the spherical angles $\Omega=\{\theta,\phi\}$. Second, if the thickness of a shell also satisfies the inequality $\mathcal{W}\mathcal{R}\ll\lambda^2$, where $\mathcal{R}$ is the shell radius and λ is the London penetration depth, the external magnetic field will be only weakly perturbed by the nanoshell.

II. VORTEX-ANTIVORTEX SEPARATION AND THE MEISSNER BELT

Bulk superconductors expel the magnetic field and form a Meissner state up to a lower critical field H_{c1}. When exposed to higher fields, type II superconductors allow the magnetic field to penetrate in the form of quantized superconducting Abrikosov vortices, up to a field H_{c2}. The behavior of superconducting nanoshells can be derived from a variational argument in which we consider a nanoshell with a vortex line along the z axis at a magnetic field $H_{c1}<H<H_{c2}$. This vortex line punctures the shell in two points, forming "cores" around which the two-dimensional (2D) superflow on the surface takes place. The 2D superflow on the northern hemisphere ($\theta<\pi/2$) rotates anticlockwise around the unit vector $\mathbf{e}_r$ at the core, whereas on the southern hemisphere ($\theta>\pi/2$) it rotates clockwise around the unit vector $\mathbf{e}_r$ at the southern core. We will refer to the local flow pattern on the northern hemisphere as a 2D vortex and to that on the southern hemisphere as a 2D antivortex. When we ramp down the magnetic field to a value $H<H_{c1}$, where the vortex state is unstable, the vortex line, still parallel to the south-north axis, is moved away from the poles (so as to expel vorticity from the system). In other words, the 2D vortex and 2D antivortex move on their respective hemispheres toward the equator. There, they can merge, and the clockwise and anticlockwise flows cancel each other out, leaving a uniform order parameter. The dynamical behavior for expelling vorticity, sketched above in a qualitative way, can be investigated more rigorously using variational calculus on the Gibbs free energy. In the case of thin shells, $\mathcal{W}\ll\lambda^2/\mathcal{R}$, the Gibbs free energy becomes

$$\Delta G=\int d\Omega\Big\{(\nabla_\Omega|\psi|)^2+|\psi|^2[\nabla_\Omega\varphi-H\sin(\theta)\mathbf{e}_\phi]^2 - 2R^2|\psi|^2\Big(1-\frac{1}{2}|\psi|^2\Big)\Big\}. \quad (1)$$

In this expression, we use spherical coordinates with the z axis parallel to the external magnetic field such that $\nabla_\Omega=\mathbf{e}_\theta(\partial/\partial\theta)+\mathbf{e}_\phi\sin^{-1}(\theta)(\partial/\partial\phi)$. Two experimentally tunable

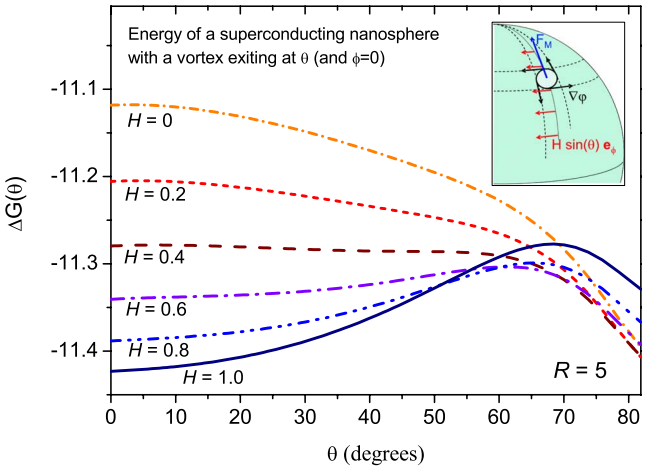

FIG. 1. (Color online) The Gibbs free energy of a vortex-antivortex pair, displaced away from the poles down to a latitude θ, is shown for different values of the applied magnetic field. The origin of the metastability barrier, which develops with increasing the applied magnetic field, is a Magnus-Lorentz F_M force pushing vortices toward the poles, as illustrated in the inset. This force arises from a differential velocity field across the vortex due to the interplay between the supercurrent of the vortex, proportional to the phase gradient $\nabla\varphi$, and the screening supercurrent induced by the magnetic field H.

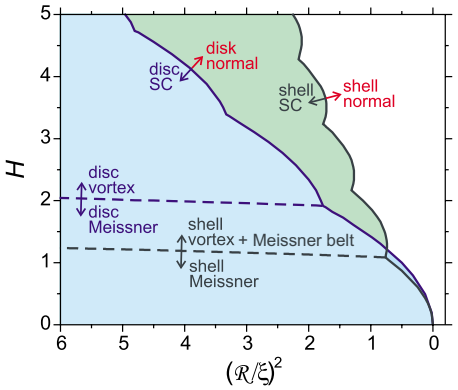

FIG. 2. (Color online) The phase diagram for a thin spherical shell is compared to that of a flat thin disk. The shaded regions show the values of magnetic field and radius where the superconducting (SC) state is supported. The solid lines correspond to the boundaries between the thermodynamically stable normal and superconducting states. The dashed lines correspond to the boundaries between the thermodynamically stable Meissner and vortex states.

parameters remain: the radius of the nanoshell and the external magnetic field. The external magnetic field $\mathcal{H}$ appears in Eq. (1) as $H=\Phi/\Phi_0=\pi\mathcal{R}^2\mathcal{H}\Phi_0$ corresponding to the amount of flux quanta of the applied field that pass through the equatorial plane of the sphere. The radius of the shell appears as $R=\mathcal{R}/(\sqrt{2}\xi)$, which is the ratio of shell radius to the coherence length multiplied by $\sqrt{2}$. To describe a vortex state, where the core of the vortex on the northern hemisphere is at $\Omega=\{\theta_v,0\}$ and the corresponding antivortex is at $\{\pi-\theta_v,0\}$ on the southern hemisphere, we use the trial wave function

$$|\psi(\theta,\phi)| = a(1-e^{-R\vartheta})(1-e^{-R(\pi-\vartheta)}),$$

$$\varphi(\theta,\phi) = \arctan\left(\frac{\sin\theta\sin\phi}{\sin\theta\cos\phi-\sin\theta_v}\right) - \arctan\left(\frac{\sin\theta\sin\phi}{\sin\theta\cos\phi-\sin(\pi-\theta_v)}\right),$$

where a is a variational parameter and

$$\cos\vartheta = \cos\theta\cos\theta_v + \sin\theta\sin\theta_v\cos(\phi).$$

As illustrated in Fig. 1, where the calculated Gibbs free energy is plotted for different values of the magnetic field and for the particular case of $R=5$, the homogeneous external magnetic field gives rise to an energy barrier that pushes the 2D vortex and the 2D antivortex away from the equator and toward the poles, separating the pair. This is in remarkable contrast with flat superconducting films in a homogeneous magnetic field, where vortex-antivortex pairs tend to annihilate. Unlike the Bean-Livingston barrier,[12] the present metastability barrier is not caused by the interaction with an image vortex but by the surface curvature. The inset of Fig. 1 illustrates the origin of the Magnus-Lorentz force, which is responsible for the separation of vortex-antivortex pairs. When multiple single vortices and antivortices are present, they aggregate at the opposite poles, forming a vortex lattice polar region.

The equatorial region remains a vortex-free "Meissner state," although a shielding current is present. The Meissner belt at the equator represents a Cooper pair reservoir tangent to the magnetic field. As shown in Ref. 13, the current-carrying capacity of superconducting strips can be enhanced by geometrical barriers, which result in the coexistence of isolated vortex-filled regions with current-carrying vortex-free Meissner regions. In the case of a nanoshell, we find that the coexistence of the Meissner belt with the vortex lattice at the poles aids superconductivity in a similar way. In Fig. 2 we compare the superconductivity phase diagram for nanoshells and disks. The results, shown in this figure and below, originate from a finite-element numerical solution of the time-dependent Ginzburg-Landau (TDGL) equation, described in Ref. 14 and applicable also to the case when magnetic fields, induced by supercurrents, are non-negligible. The set of parameters, governing the solution of the TDGL equation in Ref. 14, contains—in addition to R and H—also the ratio $\mathcal{W}\mathcal{R}/\lambda^2$. Figure 2 corresponds to the case of thin layers where $\mathcal{W}\mathcal{R}\ll\lambda^2$. As seen from Fig. 2, for nanoshells the region in the phase diagram where superconducting vortex state is present is considerably expanded; superconducting nanoshells tolerate considerably higher magnetic fields than superconducting disks.

Due to the presence of the Meissner belt, in relatively large shells not only the Meissner state but also the thermodynamically stable states with one or few quanta of vorticity are characterized by a negative magnetic moment of the shell, i.e., these states are always diamagnetic (see, e.g., Fig. 2 of Ref. 14). Our calculations show that paramagnetic states with one or few vortex pairs (or a pair of giant vortices) can be thermodynamically stable only in sufficiently small and thin shells. In Fig. 3, this is illustrated for the case $L=1$,

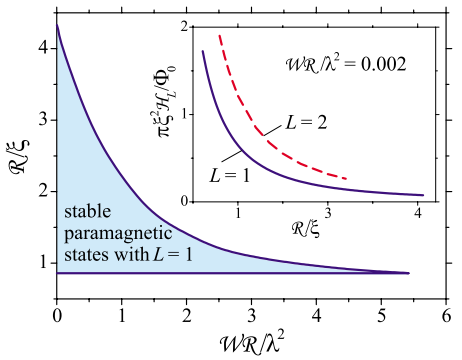

FIG. 3. (Color online) Boundaries of the region, where paramagnetic states with $L=1$ on a spherical shell of radius $\mathcal{R}$ and thickness $\mathcal{W}$ can be thermodynamically stable. Inset: magnetic fields, which correspond to the equilibrium positions of thin spherical shells with vorticity $L=1$ and $L=2$ in an inhomogeneous magnetic field, as a function of the shell radius.

where L is the number of quanta of vorticity present. For small and thin spherical shells, the magnetic fields $\mathcal{H}_L$, which correspond to the minima of the free energy for states with $L=1,2,\ldots$, lie in the range where these states are thermodynamically stable. As a result, those shells—when assumed to be able to move freely—can manifest a rather peculiar behavior in a weakly inhomogeneous magnetic field (i.e., in a field, which substantially varies only on a size scale much larger than the shell radius). Indeed, as illustrated in the inset of Fig. 3, the values $\mathcal{H}_L$ (which are almost insensitive to the shell thickness $\mathcal{W}$) strongly depend on $\mathcal{R}$. This means that shells with the same nonzero vorticity but different radius (as well as shells with the same size but different vorticity) can be spatially separated in an inhomogeneous magnetic field. In a sense, this situation is analogous to the quantized levitation, analyzed in Ref. 15 for a superconducting ring in the magnetic field of another fixed ring (of course, while for the levitating ring one should take care of keeping its orientation parallel to the fixed ring, there is no need of such a care in the case of spherically symmetric shells). The aforedescribed behavior of thin spherical nanoshells is in a remarkable contrast to the case of full spherical grains. As implied by the results,[16] based on the linearized Ginzburg-Landau equation, as well as by our calculations for the nonlinear TDGL equation, thermodynamically stable states in full spherical grains are always diamagnetic. This means that in an inhomogeneous magnetic field the thermodynamic equilibrium position of all full grains will correspond to $\mathcal{H}=0$ (or to the lowest available value of $\mathcal{H}$).

III. FLUX HYSTERESIS

Vortices can only be expelled, or nucleated, near the equator, where the metastability energy barrier is high, enabling flux hysteresis. In Fig. 4, the black solid curves show the Gibbs free energy of the ground state as a function of the magnetic field for a given shell geometry. The Meissner state is thermodynamically stable below $H\approx 1.5$, while for $1.5<H<2.85$, the state with a single vortex is stable. When the magnetic field is slowly ramped up (green dashed curve),

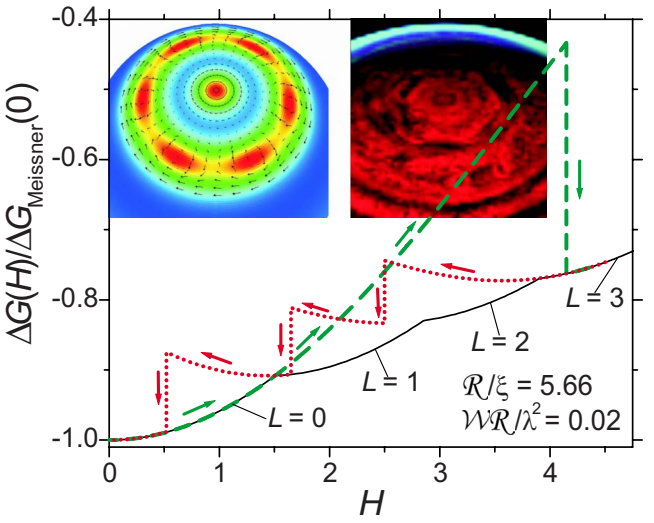

FIG. 4. (Color online) Flux hysteresis in a superconducting nanoshell. The Gibbs free-energy difference between the normal and superconducting states is plotted as a function of the magnetic field. The solid curve shows the thermodynamically stable state. The dashed (dotted) curve corresponds to a slow increase (decrease) in the applied magnetic field. Inset: on the left, a vortex pattern that arises at high magnetic field ($H=20$) when a ringlike vortex in a nanoshell with $\mathcal{R}/\xi=11.5$ and $\mathcal{WR}\ll\lambda^2$ breaks up into separate vortices. The color scale indicates the Cooper pair density from blue (dark gray background) (high) to red (gray patches) (low). The supercurrents are indicated by the arrow field. On the right, a cloud pattern observed at the north pole of Saturn (Ref. 17).

and down again (red dotted curve), a clear hysteresis effect in the vorticity is seen. Due to the metastability barrier, when the field is ramped up, the vortex line is prohibited from entering the nanoshell and vortices start nucleating at the equator only at $H\approx 4.15$ when the shell makes a transition from the Meissner state to the state with three circulation quanta. To expel all vortices from the shell, an external magnetic field has to be lowered down to $H\approx 0.5$. Our calculations show that flux hysteresis is enhanced when increasing the thickness and size of the shell; at $\mathcal{WR}\sim\lambda^2$ an external magnetic field of opposite direction should be applied in order to remove flux completely from the shell. We emphasize that here the flux is trapped not by flux pinning at imperfections but rather by the topology of the system itself. While the above simulations are performed for idealized spherically symmetric nanoshells, in realistic nanoshells, inevitable imperfections may perturb the trapping potential for vortices. In order to model the effect of those imperfections, we have considered nanoshells with spatial variations in the Ginzburg-Landau parameter κ. According to the results of our calculations, though the inhomogeneity of κ usually tends to destabilize metastable vortex states, this destabilizing effect on vortex trapping is not dramatic in the case of relatively small variations in κ. Our results imply that vortex trapping should be robust also with respect to moderate deviations of the nanoshell shape from sphericity.

The particular dynamics of vortices entering the shell is shown in Fig. 5. The distribution of supercurrents, typical for a pair of 2D vortices, appears only when the separation be-

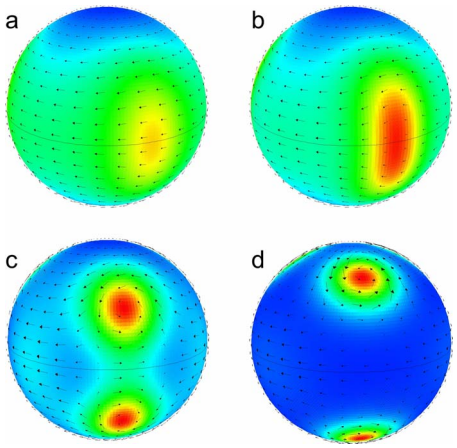

FIG. 5. (Color online) Four snapshots of the dynamical process of vortices entering a superconducting nanoshell with $\mathcal{R}/\xi=5.66$ and $\mathcal{W}\mathcal{R}/\lambda^2=0.02$ at $H=4.15$. The color scale indicates the Cooper pair density from blue (dark gray background) (high) to red (gray patches) (low). The supercurrents are indicated by the arrow field. (a) A redistribution of the Cooper pair density is already present in the Meissner state. (b) The vortices nucleate at a depression of the Cooper pair density at the equator, (c) separate into two counter-rotating two-dimensional vortices, and (d) proceed toward the poles.

tween the vortex cores is of the order of twice the coherence length. As a consequence, vortex cores can only be present outside a Meissner belt of latitudes $\pm\Delta\theta_M \approx \arctan[\xi/(2\mathcal{R})]$ around the equator. Qualitatively, this Meissner belt resembles the hurricane-free belt of 3° latitude around the Earth equator. Expressing the Ginzburg-Landau equations in hydrodynamic form, the resulting equations for superfluid velocity and Cooper pair density are formally similar to the shallow-atmosphere Euler equations used to model atmospheric dynamics.[18] As a result, there is a similarity between the behavior of atmospheric vortices (cyclones) on the macroscopic globe and superconducting vortices on the nanoshell. This is illustrated in the inset of Fig. 4 for the formation of polar vortex lattices. The lhs panel of this inset shows a vortex pattern that arises on a nanoshell when a ringlike vortex breaks up into separate vortices. The rhs panel of the inset depicts a cloud pattern observed at the north pole of Saturn. The initial axially symmetric state in the nanoshell included nonuniform vorticity[14,19] with a different angular-momentum state near the poles and near the equator. Differential wind speeds (or superconducting currents) in two bands circling the pole lead to a depression (of pressure in the atmosphere and of Cooper pair density in the superconductor) in the interface between the bands. A modulation of this depression reduces the energy in the case of a superconductor—one can speculate that a similar mechanism may be at work at Saturn's pole.

IV. CONCLUSIONS

In nanoscopic superconductors, confinement potentials and periodic modulation of material parameters have been explored as tools to manipulate flux and quantum coherence. Here, we have shown that the geometry of the sample can also be used to manipulate flux. The spherical shell geometry leads to two important properties: first, 2D-vortex-antivortex pairs tend to separate rather than annihilate, and second, the curvature enables the coexistence of a vortex state and a Meissner (nonvortex) belt close to the equator on the same surface. These properties result in a higher critical magnetic field in a shell in comparison to a disk with corresponding cross section. Also we find a pronounced hysteresis effect for flux trapping in the nanoshell, allowing magnetic separation of spheres with different vorticity in an inhomogeneous field. Experimental techniques for producing monodisperse and uniform SiO_2 nanospheres[20] that can be coated with a metal[11,21] such as niobium, either individually or in a film of hemispheres, offer the prospect to probe the enhanced magnetic properties of nanoshells discussed in the present work.

Note added in proof. The authors thank G. Williams for pointing out that curvature and topology affect the superfluid transition as well as the superconducting transition. Curvature effects in superfluids have been demonstrated in helium films adsorbed in porous materials with small grain sizes,[22] where the vortex dynamics is driven experimentally by rotation.[23–25]

ACKNOWLEDGMENTS

This work was supported by the Fund for Scientific Research-Flanders Projects under Grants No. G.0370.09N, No. G.0180.09N, No. G.0356.06, No. G.0115.06, and No. G.0435.03, the WOG under Project No. WO.033.09N, and the U.S. Department of Energy under Grant No. DE-FG02-ER45978. V.V.M. acknowledges Methusalem Funding by the Flemish Government. J.T. acknowledges financial support from the Special Research Fund of the University of Antwerp, BOF NOI UA 2004.

[1] J. I. Martin, M. Velez, J. Nogues, and I. K. Schuller, Phys. Rev. Lett. **79**, 1929 (1997).
[2] M. Lange, M. J. Van Bael, Y. Bruynseraede, and V. V. Moshchalkov, Phys. Rev. Lett. **90**, 197006 (2003).
[3] K. Harada, O. Kamimura, H. Kasai, T. Matsuda, A. Tonomura, and V. V. Moshchalkov, Science **274**, 1167 (1996).
[4] V. V. Moshchalkov, L. Gielen, M. Dhallé, C. Van Haesendonck, and Y. Bruynseraede, Nature (London) **361**, 617 (1993).
[5] M. B. Hastings, C. J. Olson Reichhardt, and C. Reichhardt, Phys. Rev. Lett. **90**, 247004 (2003).
[6] B. Y. Zhu, F. Marchesoni, and F. Nori, Phys. Rev. Lett. **92**, 180602 (2004).
[7] C. C. de Souza Silva, J. Van de Vondel, M. Morelle, and V. V. Moshchalkov, Nature (London) **440**, 651 (2006).

[8] S. B. Field, S. S. James, J. Barentine, V. Metlushko, G. Crabtree, H. Shtrikman, B. Ilic, and S. R. J. Brueck, Phys. Rev. Lett. **88**, 067003 (2002).
[9] M. Bowick, A. Cacciuto, D. R. Nelson, and A. Travesset, Phys. Rev. Lett. **89**, 185502 (2002).
[10] M. Bowick, H. Shin, and A. Travesset, Phys. Rev. E **75**, 021404 (2007).
[11] R. D. Averitt, D. Sarkar, and N. J. Halas, Phys. Rev. Lett. **78**, 4217 (1997).
[12] C. P. Bean and J. D. Livingston, Phys. Rev. Lett. **12**, 14 (1964).
[13] E. Zeldov, A. I. Larkin, V. B. Geshkenbein, M. Konczykowski, D. Majer, B. Khaykovich, V. M. Vinokur, and H. Shtrikman, Phys. Rev. Lett. **73**, 1428 (1994).
[14] V. N. Gladilin, J. Tempere, I. F. Silvera, J. T. Devreese, and V. V. Moshchalkov, Phys. Rev. B **77**, 024512 (2008).
[15] S. B. Haley and H. J. Fink, Phys. Rev. B **53**, 3497 (1996).
[16] B. J. Baelus, D. Sun, and F. M. Peeters, Phys. Rev. B **75**, 174523 (2007).
[17] Cassini mission image credit: NASA, JPL, University of Arizona.
[18] D. R. Durran, *Numerical Methods for Wave Equations in Geophysical Fluid Dynamics* (Springer, Berlin, 1999).
[19] Hu Zhao, V. M. Fomin, J. T. Devreese, and V. V. Moshchalkov, Solid State Commun. **125**, 59 (2003).
[20] W. Stober, A. Fink, and E. Bohn, J. Colloid Interface Sci. **26**, 62 (1968).
[21] P. Jiang, J. F. Bertone, K. S. Hwang, and V. L. Colvin, Chem. Mater. **11**, 2132 (1999).
[22] V. Kotsubo and G. Williams, Phys. Rev. B **33**, 6106 (1986).
[23] M. Fukuda *et al.*, J. Low Temp. Phys. **113**, 417 (1998).
[24] C. Wang and L. Yu, Phys. Rev. B **33**, 599 (1986).
[25] D. J. Bishop, J. E. Berthold, J. M. Parpia, and J. D. Reppy, Phys. Rev. B **24**, 5047 (1981).